Available online at www.sciencedirect.com
ScienceDirect
C. R. Physique 9 (2008) 804–815
COMPTES RENDUS PHYSIQUE
http://france.elsevier.com/direct/COMREN/

Recent advances in quantum dot physics / Nouveaux développements dans la physique des boîtes quantiques

Optics with single nanowires

V. Zwiller [a,*], N. Akopian [a], M. van Weert [a], M. van Kouwen [a], U. Perinetti [a], L. Kouwenhoven [a], R. Algra [b,c,d], J. Gómez Rivas [e], E. Bakkers [c], G. Patriarche [f], L. Liu [f], J.-C. Harmand [f], Y. Kobayashi [g], J. Motohisa [g]

[a] *Quantum Transport, Kavli Institute of Nanoscience, Delft University of Technology, 2628CJ Delft, The Netherlands*
[b] *Materials Innovation Institute (M2i), 2628CD Delft, The Netherlands*
[c] *Philips Research Laboratories Eindhoven, High Tech Campus 11, 5656AE Eindhoven, The Netherlands*
[d] *IMM, Solid State Chemistry, Radboud University Nijmegen, Heijendaalseweg 135, 6525AJ Nijmegen, The Netherlands*
[e] *FOM Institute for Atomic and Molecular Physics, c/o Philips Research Laboratories Eindhoven, High Tech Campus 4, 5656 AE Eindhoven, The Netherlands*
[f] *Laboratoire de Photonique et de Nanostructures, CNRS, route de Nozay, 91460 Marcoussis, France*
[g] *Graduate School of Information Science and Technology, Hokkaido University, North 14, West 9, Sapporo 060-0814, Japan*

Abstract

Semiconducting nanowire heterostructures represent a new class of nanostructures that offer unprecedented freedom in material design. The position, diameter, composition and doping can be controlled with precision and complex structures such as core-shell and branched wires have already been demonstrated. Here we show that heterostructures in nanowires can define quantum emitters and that single spins can be addressed optically. We also present results on electrically contacted nanowires. The operation of single nanowires as light emitting diode or photodetector is demonstrated. ***To cite this article: V. Zwiller et al., C. R. Physique 9 (2008).***

Résumé

Optique avec des nanofils uniques. Les nanofils semiconducteurs hétérostructurés constituent une nouvelle classe de nanostructures, qui offrent une souplesse de conception sans précédent. La position, le diamètre, la composition et le dopage de ces nanofils peuvent être contrôlés avec précision, et des structures complexes – tels que les nanofils « cœur-coquille » ou des structures arborescentes à nanofils ont déjà été réalisées. Nous montrons dans cet article la possibilité de réaliser des émetteurs quantiques, et d'adresser optiquement un spin unique confiné au sein d'un nanofil. Nous présentons par ailleurs des résultats obtenus sur des nanofils contactés électriquement. Nous montrons qu'il est possible de réaliser une diode électroluminescente ou encore un photodétecteur à partir d'un nanofil unique. ***Pour citer cet article : V. Zwiller et al., C. R. Physique 9 (2008).***

Keywords: Nanowire; Quantum emitter

Mots-clés : Nanofil ; Émetteur quantique

* Corresponding author.
E-mail address: v.zwiller@tudelft.nl (V. Zwiller).

1631-0705/$ – see front matter
doi:10.1016/j.crhy.2008.10.016

1. Introduction

Nanowires are defined as structures that have an unconstrained longitudinal size while lateral size is restricted to tens of nanometers or less. At these scales, quantum mechanical effects become important — hence such wires are also known as "quantum wires" [1]. Many different types of nanowires exist today, including metallic (e.g., Ni, Pt, Ag, Au), semiconducting (e.g., Si [2], InP [3], InAs [4], GaAs [5,6], GaN [7]), and dielectric (e.g., SiO_2,TiO_2) ones. Typical nanowires exhibit aspect ratios (length-to-width ratio) of 100 or more. As such, they are often referred to as one-dimensional materials.

There are many applications where nanowires may become important. They could be used to interconnect or to address components into extremely small circuits. They could become the future building blocks of electronics, opto-electronics, nanoelectromechanical devices and biomolecular nanosensors. They also have potential as field-emitters or as additives in advanced composite nanosensors. The nanowires that we study are fabricated via "bottom-up" methods in contrast to techniques based on etching. To create active *electronic* elements, a key step is to chemically dope a semiconductor nanowire to create p-type and n-type regions [8]. The next step is to create a p-n junction, one of the simplest electronic devices. This can be achieved in two ways. The first way is to simply physically cross a p-type wire and an n-type wire [8]. The second method involves chemically doping a single wire with different dopants along the length [9]. The last method can create a p-n junction within a single wire.

To create active *photonic* elements, a key step is to incorporate a single quantum dot in a nanowire [10]. Semiconductor quantum dots are well known sources of single [11–13] and entangled photons [14–16] and are naturally integrated with modern semiconductor electronics. The most popular fabrication technique is to exploit the Stranski–Krastanow growth mode, where strain is the driving force leading to self-assembled quantum dots formation [17,18]. In comparison, the fabrication of quantum dots in semiconducting nanowires does not need strained material systems and it brings additional unique features. It provides easiness in the manipulation of a single quantum dot; this single dot can then be electrically addressed via an inherent one-dimensional channel for charge carriers: the nanowire. In addition, the natural alignment of vertically stacked quantum dots allows designing quantum dot molecules. Furthermore, the unprecedented material and design freedom makes them very attractive for novel opto-electronic devices and quantum information processing.

Access to intrinsic spin and polarization properties of a quantum dot in a nanowire is challenging because of the limited quality of nanowire quantum dots, partly because the quantum dot is located very close to the sample surface. Moreover, the nanowire geometry strongly affects the polarization of photons emitted or absorbed by a nanowire quantum dot, and is thus an important obstacle for applications based on intrinsic spin or polarization properties of quantum dots such as electron spin memory or generation of entangled photons. Indeed, it has been shown that photoluminescence of homogeneous nanowires is highly linearly polarized with a polarization direction parallel to the nanowire elongation [19].

In this article we present our recent progress in understanding the physical properties of single nanowires, single nanowire quantum dots and nanowire based devices. We first describe several growth techniques that are used to grow optically active nanowire quantum dots of good quality with narrow emission lines, enabling us to access the spin properties of the exciton. We also demonstrate that a single nanowire containing a pn junction can be operated as a light emitting diode (LED), as well as a photodetector.

2. Nanowire growth

Nanowires can be fabricated in numerous ways. Metallic nanowires are usually synthesized in suspension. Silicon nanowires can be etched from a silicon-on-insulator wafer, using conventional complementary metal–oxide–semiconductor (CMOS)-compatible techniques. Contrary to this top-down approach, a bottom-up approach based on the Vapor–Liquid–Solid (VLS) synthesis method, may be used to grow semiconductor nanowires. Since the first demonstration of this method in 1964 [20], it has been investigated, analyzed and improved by several groups [21–25]. The VLS method can be implemented with several growth techniques such as vapor phase epitaxy (VPE) [20,21], laser ablation [23], metal-organic vapor phase epitaxy (MOVPE) [22], chemical beam epitaxy (CBE) [24], and molecular beam epitaxy (MBE) [25]. Nanowires of Si/Ge, III-V or II-VI compounds have been fabricated. The process starts with the deposition of metallic particles, usually nanometer sized gold particles, on the substrate before growth. These nano-particles can act as chemical or physical catalysts. At growth temperature, they generally form liquid droplets

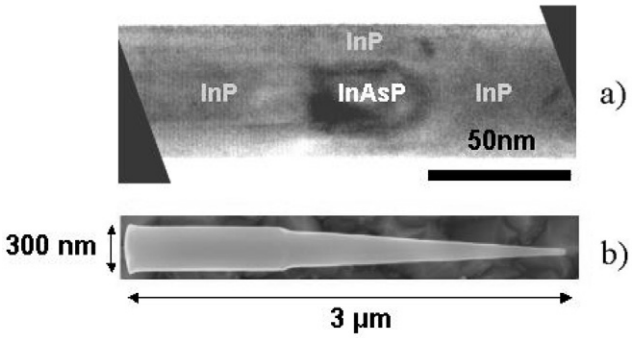

Fig. 1. (a) Transmission electron microscope (TEM) image of a segment of $InAs_{0.24}P_{0.76}$ (diameter 22 nm, length 40 nm) in an InP nanowire. A 20 nm InP shell was deposited at lower temperature on the sidewalls of the initial core. (b) Scanning electron microscope (SEM) image of a thicker shell grown to obtain diameters equal to a fraction of the emitted wavelength. Structures grown by MBE in the Harmand group.

with the semiconductor constituents. When the sample is exposed to a supersaturated vapor flow of source materials, the concentration of these constituents in the liquid phase increases until they condensate at the droplet/substrate interface: the nanowires grow. The chemical catalyst effect consists in the preferential decomposition of precursor materials, such as organo-metallics used in MOVPE, at the surface of the metal droplets. The growth rate is then locally enhanced because free constituents are more abundant near the droplets [26]. This is the dominant mechanism for nanowire growth by MOVPE. However, this effect does not operate in MBE where elemental constituents are supplied to the sample. In that case, the faster nucleation rate at the droplet/substrate interface results from a physical catalytic effect: the periphery of the droplet, boundary between the 3 phases, vapor, liquid and solid, presents a lower energy barrier to the nucleation [27]. This effect also leads to nanowire formation. In both cases, the final nanowire length can be adjusted by controlling the growth time, while the diameter is set by the catalyst particle size. Compound nanowires with superlattices of alternating materials can be created by switching sources during growth. In this respect, switching group V rather than group III sources is preferable in Au-assisted growth. This is because Au droplets mainly alloy with group III elements whilst the solubility of group V elements remains very low. Therefore, forming abrupt interfaces between two different compounds is more straightforward if they contain the same group III constituent. In fact, the realization of axial heterostructures by VLS has been most successful in systems like GaP/GaAsP [28] or InP/InPAs [24,29].

An alternative approach to nanowire synthesis relies on catalyst-free growth modes. Under specific conditions, the growth of particular compounds such as GaN or ZnO can spontaneously deviate from a conventional two-dimensional regime to the formation of nanocolumns [30,31]. One advantage is that catalyst-free synthesis excludes the possible incorporation of catalyst metallic impurities in the nanowires. For heterostructure formation, this growth mode also provides better control of the element commutation, since it is not dependent on a complex interaction between the constituents in the vapor phase, the metallic catalyst and the semiconductor solid phase. Similar advantages can be obtained for a larger variety of compounds by using masked substrates and conditions leading to a selective growth in the apertures [32].

Nanowire geometry offers further original possibilities to fabricate heterostructures: growth conditions can be varied in order to switch from axial growth, promoted by the catalytic effects explained above, to radial growth where material nucleates on the nanowire sidewalls. This process results in core-shell heterostructures [33] of particular interest to shield an active core region by a high bandgap shell material. For instance, Fig. 1(a) shows a TEM image of an InAsP segment in an InP nanowire with an InP shell [29], in (b) a SEM view of a nanowire with a large InP shell is shown.

An additional advantage of nanowires over conventional two-dimensional growth is the flexibility in structuring highly lattice-mismatched material systems: because of the very small diameter, strain can relax along the nanowire sidewalls without introducing dislocations at the mismatched interfaces, increasing the choice of material combinations as compared to two dimensional growth. This advantage may however be limited in radial heretostructures, where the core can be strained by the shell.

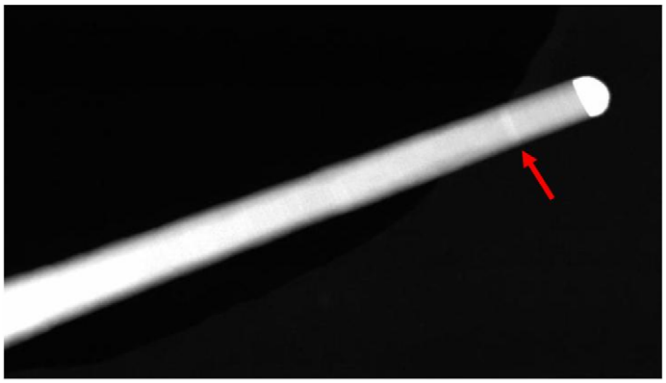

Fig. 2. TEM image of an InP nanowire with an InAsP section. The gold catalyst is visible on top of the wire, the arrow points at the InAsP segment. MOVPE grown samples by the Bakkers group.

The crystal structure in nanowires can be zinc-blende as for usual bulk III-V materials, but very often the wurtzite structure is found to dominate. This could be seen as another advantageous flexibility over two dimensional growth, at least when the perfect control of this crystalline phase via growth parameters will be demonstrated.

The growth of branched nanowires where catalyst particules have been deposited on a nanowire before a second growth stage was also demonstrated [34]. This technique opens the way to complex three dimensional device architectures.

In the following we describe the fabrication of nanowires by three different techniques: MOCVD and MBE growth performed with gold nanoparticles as catalysts and MOCVD growth on masked substrate.

2.1. Metal organic phase epitaxy with gold catalysts

For some of our experiments we used single $InAs_{0.25}P_{0.75}$ quantum dots embedded in InP nanowires, grown by metal-organic vapor-phase epitaxy [35]. Colloidal gold particles of 20 nm diameter were deposited on a (111)B InP substrate as catalysts for vertical nanowire growth. The nanowires were grown at a temperature of 420 °C, using phosphine (PH_3) and trimethylindium (TMI) as precursors. After 10 minutes of InP growth, an InAsP section was grown by introducing arsine (AsH_3) into the reactor. The fraction of As in the InAsP section was controlled by the ratio between the molar fractions of PH_3 and AsH_3. After 2 seconds of InAsP growth, the AsH_3 flow was stopped and 10 minutes of InP growth was continued. Subsequently a thin InP shell of 40 nm was grown around the quantum dot by raising the temperature to 600 °C. This shell passivates the surface of the quantum dot. The diameters of the nanowire and the quantum dot were controlled by the gold particle size, while the nanowire density was set by the gold particle density on the substrate. The quantum dot height and nanowire length were determined by the growth time. By controlling diameter, height and As concentration one can tune the quantum dot emission over a wide range of wavelenghts from 900 nm to 1.6 μm. Under the growth conditions described previously, we have been able to grow a sample with low density of nanowires containing a single quantum dot that emits around 950 nm. In Fig. 2, we show a high angle annular dark field transmission electron microscope (HAADF TEM) image of a nanowire quantum dot grown by MOVPE by the Bakkers group. The quantum dot is 9 nm high with a diameter of 31 nm, determined by energy dispersive X-ray analysis in a TEM. Both nanowire and quantum dot have a wurtzite crystal structure. To simplify TEM studies, the InP section following quantum dot growth was kept short, while for the samples used in our experiments, the quantum dot was centered in the nanowire.

2.2. Masked growth

Masked growth enables a definition of the nanowires positions and diameters by electron beam lithography. This approach can generate regular arrays of nanowires [33]. In addition, this technique does not require any gold for catalysis and therefore does not present any risk of material contamination by gold impurities. However, it is worth noting that the diameter of free-standing nanowires obtained by this technique are significantly larger than what can

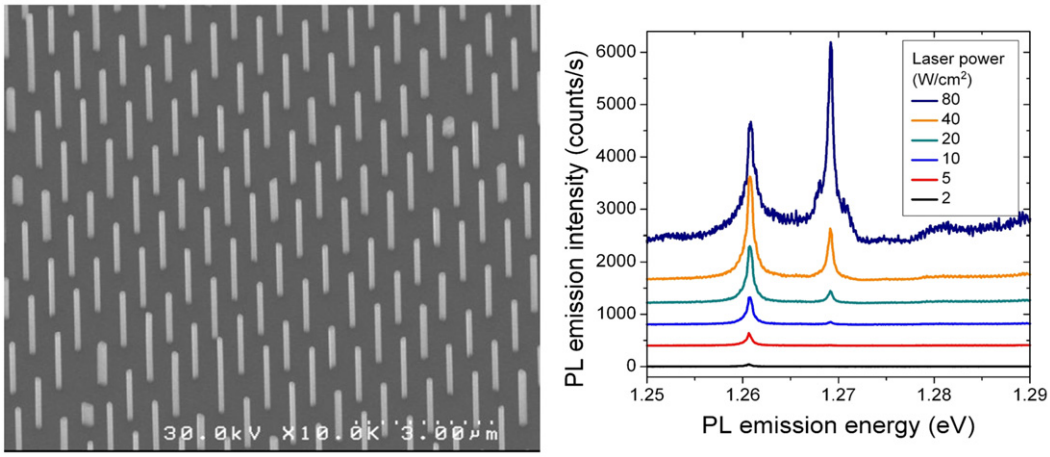

Fig. 3. (a) SEM image of a nanowire array grown by patterned MOVPE. (b) Optical spectra of a single nanowire measured at 4.2 K under 532 nm excitation. Sample grown by the Motohisa group.

be ultimately obtained by catalyst-assisted growth, as the diameter is set by the electron beam lithography resolution. Fig. 3(a) shows a scanning electron microscope image of InP nanowires grown in the Motohisa group by MOVPE on an InP substrate coated with a SiO_2 layer where holes in the SiO_2 were opened by electron beam lithography and etching, so as to obtain a regular array of uniform nanowires. Fig. 3(b) shows microphotoluminescence spectra taken at 5 K on a single nanowire containing a quantum dot. Regular arrays of nanowires containing optically active quantum dots can be grown.

2.3. Molecular beam epitaxy

Growth by Molecular Beam Epitaxy (MBE) has been performed by the Harmand group. Nanowires were grown on InP (111)B substrates in an MBE system equipped with solid sources supplying indium atoms and cracker As and P sources to produce dimers [29]. The substrate surface was first deoxidized at 530 °C, a 100 nm thick InP buffer layer was then grown to achieve an atomically flat surface. A total amount of gold equivalent to a 1 nm layer was deposited under phosphorus flux at 420 °C using a gold effusion cell installed directly into the III–V growth chamber. This procedure results in the formation of droplets containing gold alloyed with the substrate constituents. The typical distribution of droplet sizes ranges between 30 and 40 nm. After this stage, the nanowire growth was initiated by opening the In shutter. For all samples, the nominal growth rate (i.e., the growth rate on a clean and Au-free InP surface) was fixed at 0.2 nm/s. For InP/InAsP/InP heterostructure formation, the growth started with 20 min of InP, the As source was then opened for 30 s to form an InAsP segment. The As to P flux ratio was varied from sample to sample to investigate different alloy compositions. The growth was completed with 5 min deposition of InP. No growth interruption was performed at the heterointerfaces.

3. Optical properties

We study the optical properties of samples grown by the techniques described above. We concentrate on InP nanowires including InAsP segments with heights shorter than 10 nm to produce systems with a quantum dot like behavior. The emission linewidth at 4.2 K is close to our spectrometer resolution (30 µeV). The excitation power dependence reveals a clear exciton–biexciton behavior.

Fig. 4 shows optical and structural studies performed on the same single nanostructure. The nanowires were grown by MBE and transferred to a TEM grid. The TEM grid was then loaded in a helium cryostat and optical measurements were performed at 5 K. Fig. 4(a) shows a micro-photoluminescence image with a white light background where individual luminescing nanowires appear as bright spots. A spectrum taken on a single nanowire is shown in Fig. 4(b). TEM studies were then performed on the same nanowire: Fig. 4(c) shows the nanowire, Fig. 4(d) shows the InAsP/InP heterostructure at the origin of the emission shown in Fig. 4(b). This unique ability to combine optical studies and structural studies on the same single nanostructure enables the correlation of the photoluminescence properties to the

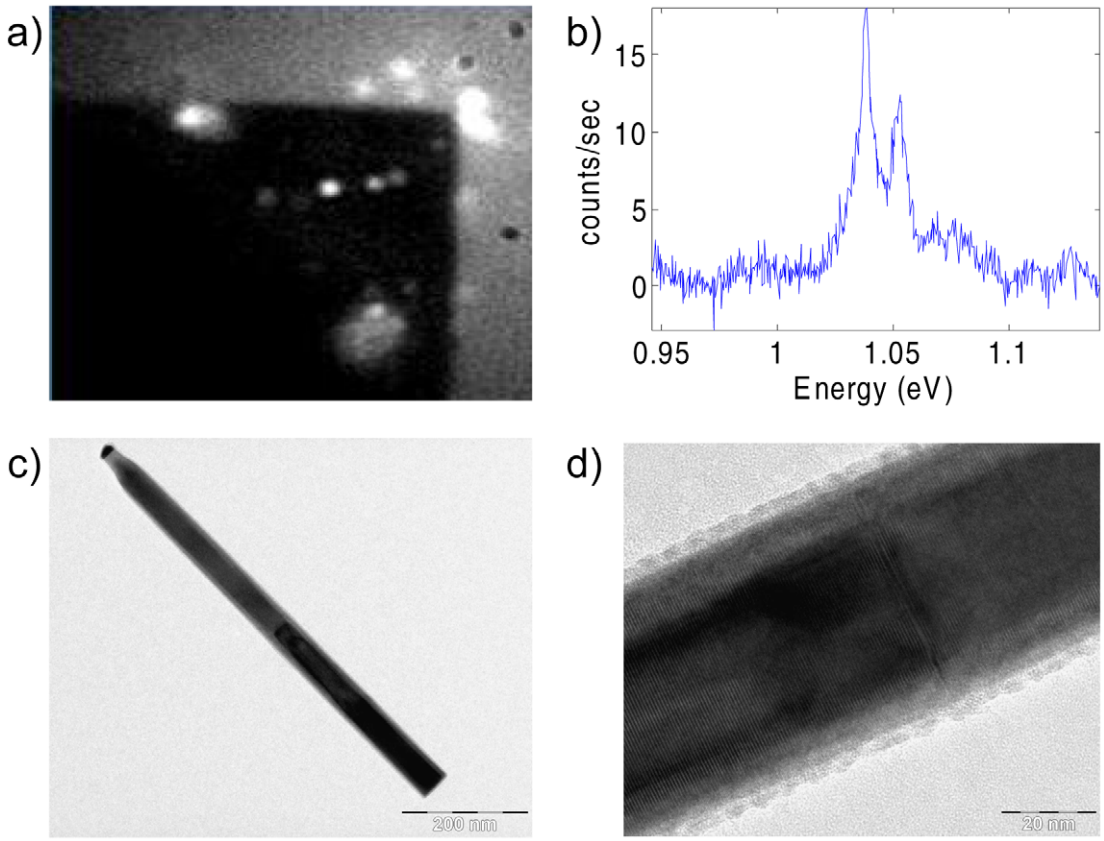

Fig. 4. (a) Micro photoluminescence image of nanowires (bright spots) on a TEM grid. (b) Photoluminescence spectrum from an InAsP section in a nanowire on the TEM grid measured at 5 K under 532 nm excitation. (c) TEM image of the nanowire studied optically in (b). (d) High resolution image of the nanowire heterostructure shown in (c). MBE grown samples by the Harmand group.

exact crystalline structure of the emitter. This kind of study is of particular relevance for nanowires that are known to present the wurtzite or the zinc-blende structure, depending on the growth conditions. Stacking faults are also commonly observed, more particularly at the proximity of heterointerfaces. These structural characteristics have a direct impact on the photoluminescence properties and can be studied through the structural and optical studies of the same quantum dot.

Fig. 5 shows an excitation power dependence of the photoluminescence from a single nanowire grown by MBE. The narrow emission (120 μeV FWHM) at a wavelength of 1.4 μm demonstrates that this type of nanostructures can emit at telecom wavelengths.

In Fig. 6(a) we show a typical excitation power dependence revealing a usual exciton–biexciton behavior and a p-shell at 30 meV higher energy. The insert shows the narrowest emission we have observed to date with a FWHM of 31 μeV, limited by our spectral resolution. The integrated photoluminescence intensities of the exciton and biexciton as a function of excitation power, represented in Fig. 6(b), show that the exciton (biexciton) increases linearly (quadratically) with excitation power and saturates at high excitation powers. This behavior is typical for the exciton and biexciton under continuous excitation.

The observation of narrow emission lines demonstrates the possibility of defining a clean system. The geometry of the nanowire however leads to a strong linear polarization. To investigate the ability to inject and extract any polarization in a nanowire quantum dot, we studied both lying (transferred to a silicon substrate covered with a 500 nm thick silica layer) and standing nanowires (on the substrate, as grown) [19]. Fig. 7(a) shows a histogram of the degree of linear polarization of the quantum dot emission and absorption for lying and standing orientations. For the lying nanowires, we observe a strong polarization along the elongation of the nanowire, whereas standing nanowires reveal weak polarization.

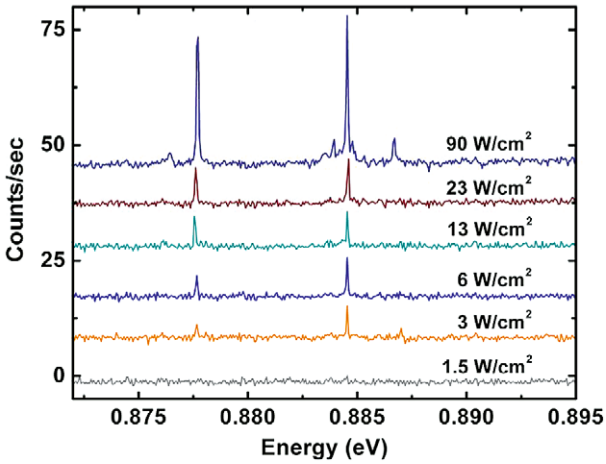

Fig. 5. Photoluminescence spectra of a single InAsP segment in an InP nanowire grown by MBE measured at 4.2 K under 532 nm excitation.

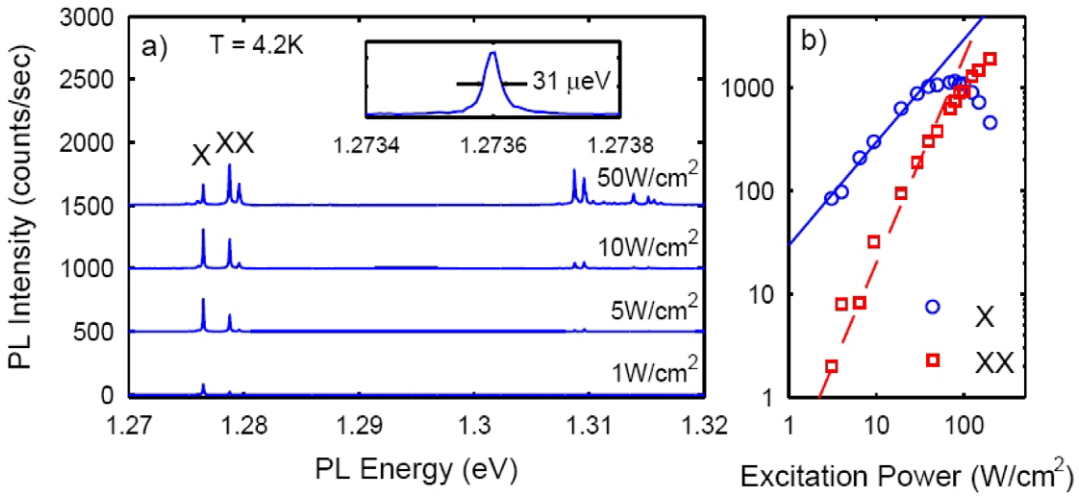

Fig. 6. (a) Power dependence of the photoluminescence from a single quantum dot in a nanowire under continuous excitation at 532 nm. (b) Integrated power dependence of two narrow emission lines attributed to the exciton and biexciton. Samples grown by the Bakkers group.

To explain our experimental results for absorption by a lying nanowire quantum dot, we use Mie theory for light scattering on dielectrics of cylindrical shape. The nanowire is modeled as an infinite cylinder. This approximation is valid as long as the nanowire diameter is much smaller than its length, as in our case. We calculate the scattering and absorption of light using the scalar wave equation in cylindrical coordinates. We consider two cases: incident electric field parallel or perpendicular to the nanowire elongation. We extract the scattered field for both polarizations from the wave equation, using the boundary conditions at the interface of two different dielectrics, i.e., at the nanowire surface. From this field, we calculate for both cases the cross-sections Q_{sca} and Q_{ext} for scattering and extinction. The absorption cross section is obtained by $Q_{\text{abs}} = Q_{\text{ext}} - Q_{\text{sca}}$ for both polarizations. To take into account the illumination of the nanowire through a microscope objective, we integrate the average absorption cross section over angles of incidence with respect to the nanowire elongation comprised between arccos (NA) and $\pi/2$. Mie theory assumes the surrounding of the nanowire as a homogeneous medium, which differs from our situation where the nanowire is lying on a substrate. Therefore, to approximate the effect of the substrate we consider the nanowire as being embedded in a medium with an effective refractive index, i.e., an average of the refractive indices of the different media surrounding the nanowire: vacuum, SiO_2 and Si. The outcome of the calculations, assuming an effective refractive index of $n_{\text{eff}} = 1.85 = 0.5n_{\text{vacuum}} + 0.25n_{SiO_2} + 0.25n_{\text{Si}}$ is represented by the dashed curve in Fig. 7(b). As an upper limit we consider the nanowire in vacuum, thus ignoring the substrate, which is represented by the solid curve in Fig. 7(b). For the

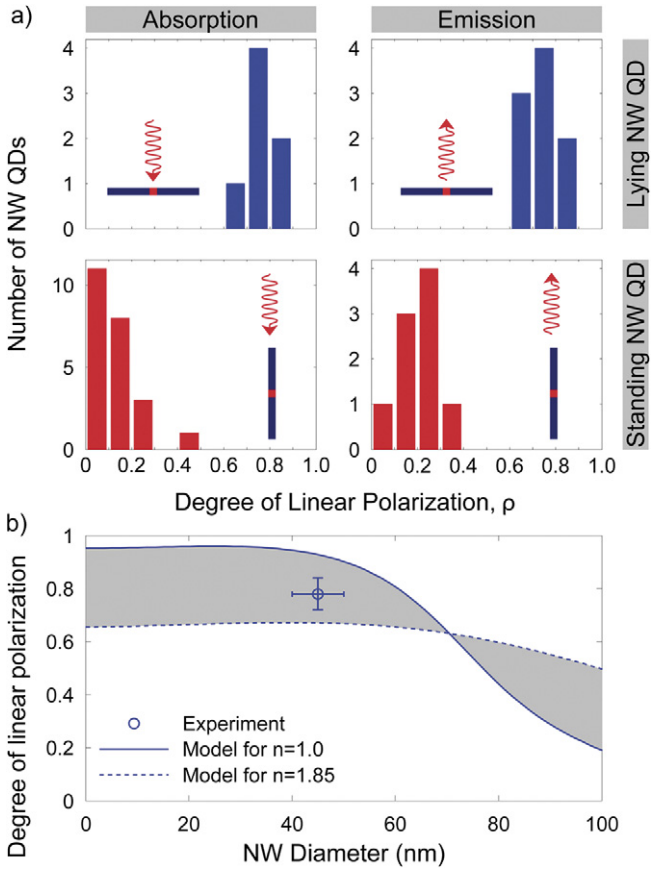

Fig. 7. (a) Statistics of the degree of linear polarization for lying and standing nanowire quantum dots. The lying nanowires (blue) show a high degree of linear polarization, about 80% and 70%, for absorbed and emitted light, respectively. The degree of linear polarization is low for standing nanowires (red), about 10% and 20% for absorbed and emitted light, respectively. Insets illustrate the nanowire orientations with respect to the light direction. (b) Calculated degree of linear polarization in non-resonant absorption as a function of nanowire diameter. In this case incident light is directed perpendicular to the nanowire elongation, as for the lying nanowire quantum dots. For the solid (dashed) curve an effective refractive index of $n = 1$ ($n = 1.85$) is used.

calculations we use our actual excitation wavelength of 532 nm. Our experimental value lies in between the two curves, having a surrounding refractive index consisting of a mixture of vacuum, Si, and SiO_2. As can be seen in Fig. 7(b) one can increase the degree of linear polarization by measuring nanowire quantum dots in vacuum, or decrease it by increasing the nanowire diameter. However, in the latter case the advantage of the one-dimensional channel of the device is reduced as well. The nanowire geometry is not the only source of polarization anisotropy. Calculations by Niquet and Mojica [36] show that the polarization properties are strongly affected by the aspect ratio of the quantum dot dimensions, due to strain originating from the lattice mismatch between the nanowire and the quantum dot. However, in our case the strain is negligible due to the low phosphorus content and the main contribution to polarization anisotropy stems from the nanowire geometry.

3.1. Zeeman splitting

Standing nanowires enable the extraction of any polarization with equal probability. This enables the observation of Zeeman splitting, provided that the emission linewidth is narrow enough. In Fig. 8(c) we show a magnetic field dependence of the exciton emission measured on a standing InP nanowire containing an InAsP quantum dot. The nanowire was grown by MOVPE using colloidal gold particles as catalysts by the Bakkers group. Polarization studies at 9 T show circular polarization (Fig. 8(b)) and no linear polarization (Fig. 8(a)).

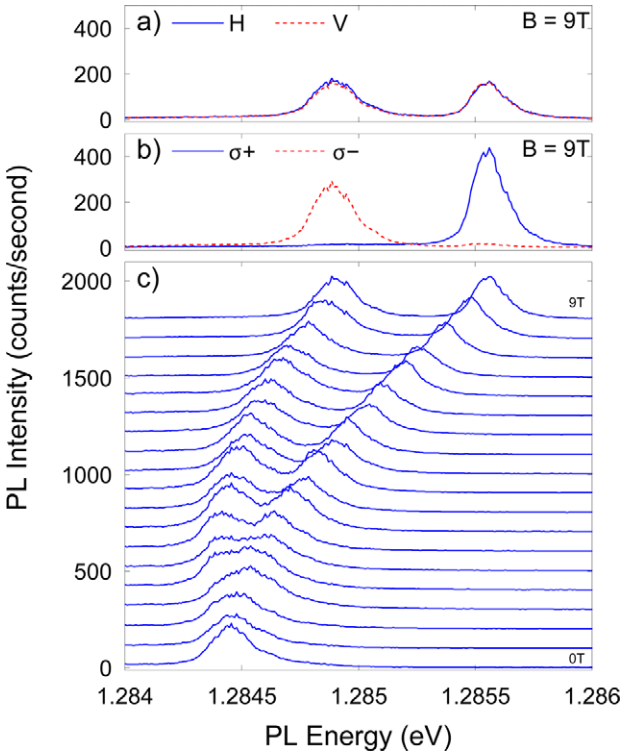

Fig. 8. (a) and (b) Polarization sensitive photoluminescence of a standing nanowire quantum dot at 9 T. The solid (dashed) curve in (a) represents vertical (horizontal) linearly polarized exciton emission, denoted by H (V). The solid (dashed) curve in (b) represents left- (right-) hand circularly polarized exciton emission. (b) PL of a standing nanowire quantum dot under external magnetic field. Magnetic field is varied between 0 and 9 T in steps of 0.5 T. Sample grown by the Bakkers group.

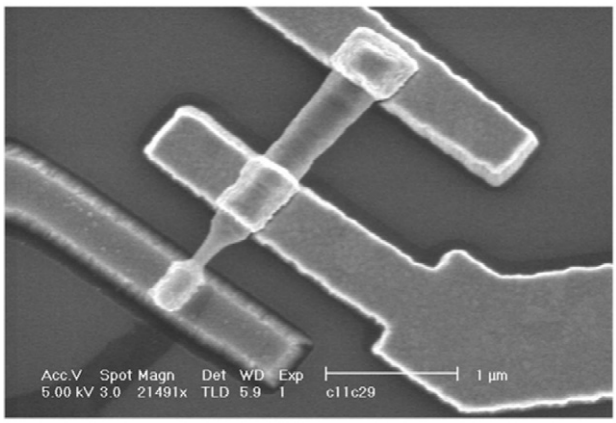

Fig. 9. SEM image of a contacted nanowire light emitting diode. Nanowire grown by the Bakkers group.

4. Nanowire devices for opto-electronics

Nanowires offer the unique opportunity of merging optics at the single photon level with transport measurements at the single electron level. A heterostructure quantum dot in a nanowire can be electrically addressed very efficiently: all the current flowing through the nanowire will necessarily flow through the quantum dot. This enables devices that would efficiently convert single electrons into single photons. To this end, we have fabricated nanowires containing pn junctions and realized nano-LEDs. The addition of an optically active quantum dot in the pn junction then yields a

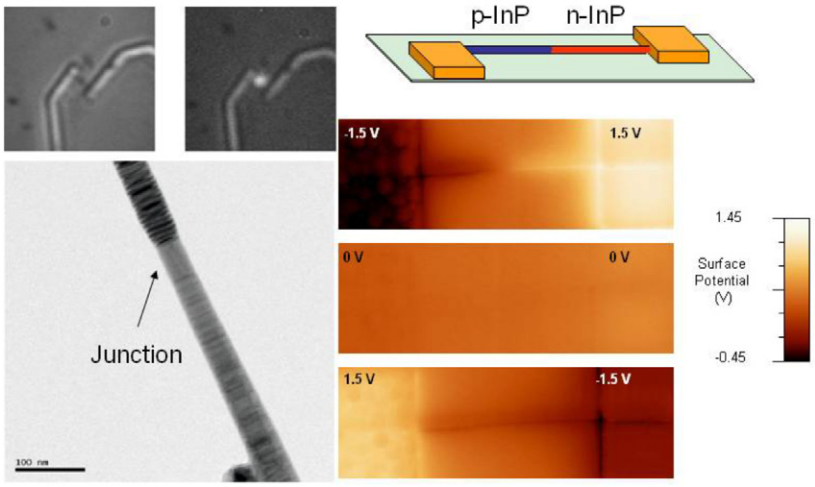

Fig. 10. Single nanowire light emitting diode. Left: microscope image of the nanowire LED without and with forward bias. Bottom left: TEM image of a pn junction in an InP nanowire. Right: electrostatic force measurements under forward (top) and reverse (bottom) bias.

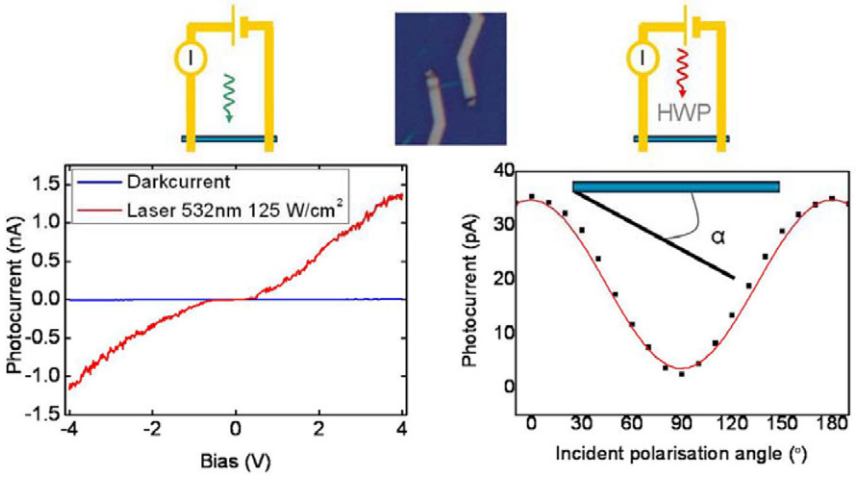

Fig. 11. Photocurrent measurement on a single nanowire. Left: photocurrent as a function of applied bias. Right: photocurrent as a function of laser polarization.

single photon LED. Such a device could coherently transfer an electron spin to the photon polarization, an important and yet missing function for quantum information processing that would link optics based long distance quantum communication with quantum information processing based on single spin manipulation [37].

4.1. Light emitting nanowire diodes

One challenge is to obtain good ohmic contacts to the p doped side of a nanowire LED. Fig. 9 shows a pn junction nanowire with two contacts on the p side (top region) made to evaluate the quality of the ohmic contacts. In Fig. 10 the device-layout, the nanowire LED emission and the electrostatic potential distribution along the device are shown. The junction is readily visible by transmission electron microscopy, the modification in doping brings about a modification of the nanowire diameter. Electrostatic force measurements are shown on the right of Fig. 9, under a reverse bias of 1.5 V, a prominent drop in potential is observed at the expected position of the pn junction. Under zero and 1.5 V forward bias, no potential drop is observed on the pn junction, this demonstrates the presence of a pn junction in the contacted nanowire and shows that the contacts are ohmic.

4.2. Photodetection

An electrically contacted nanowire can also be used for photodetection, as shown in Fig. 11. Fig. 11 left shows the photocurrent intensity as a function of applied bias in the dark and under illumination. Fig. 11 right shows the polarization dependence of the photocurrent for a lying nanowire as a function of the laser linear polarization angle. The observed photocurrent polarization is in agreement with the polarization ratio measured by photoluminescence.

5. Summary

We have shown that optically active quantum dots of good quality with sharp emission linewidth, as narrow as 30 μeV, can be defined in nanowires. In addition, doping and electrical contacts enable the fabrication of optoelectronic devices where one and only one quantum dot is contacted. The extraction of any polarization orientation is made possible with vertical nanowire devices. Quantum dots in nanowires offer important new functionalities over the well known self-assembled quantum dots such as the merging of single electron transport with single photon optics.

Acknowledgement

The work of JGR was supported by the Netherlands Foundation "Fundamenteel Onderzoek der Materie (FOM)" and the "Nederlandse Organisatie voor Wetenschappelijk Onderzoek (NWO)".

References

[1] H. Sakaki, Jpn. J. Appl. Phys. 19 (1980) L735–L738.
[2] Y. Cui, C. Lieber, Science 291 (2001) 851–853.
[3] E. Bakkers, J. van Dam, et al., Nature Mat. 3 (11) (2004) 769–773.
[4] C. Fasth, A. Fuhrer, et al., Nano Lett. 5 (7) (2005) 1487–1490.
[5] T. Sato, K. Hiruma, M. Shirai, K. Tominaga, K. Haraguchi, T. Katsuyama, T. Shimada, Appl. Phys. Lett. 66 (1995) 159.
[6] T. Katsuyama, K. Ogawa, M. Koguchi, H. Kakibayashi, G.P. Morgan, Appl. Phys. Lett. 59 (1991) 431.
[7] J.C. Johnson, H.J. Choi, et al., Nature Mat. 1 (2) (2002) 106–110.
[8] O. Hayden, R. Agarwal, et al., Nature Mat. 5 (5) (2006) 352–356.
[9] E.D. Minot, F. Kelkensberg, M. van Kouwen, J.A. van Dam, L.P. Kouwenhoven, V. Zwiller, M.T. Borgstrom, O. Wunnicke, M.A. Verheijen, E.P.A.M. Bakkers, Nano Lett. 7 (2) (2007) 367–371.
[10] M.T. Borgstrom, V. Zwiller, E. Muller, A. Imamoglu, Nano Lett. 5 (7) (2005) 1439–1443.
[11] P. Michler, A. Kiraz, C. Becher, W.V. Schoenfeld, P.M. Petroff, Lidong Zhang, E. Hu, A. Imamoglu, Science 290 (2000) 2282.
[12] E. Moreau, I. Robert, J.M. Gérard, I. Abram, L. Manin, V. Thierry-Mieg, Appl. Phys. Lett. 79 (2001) 2865.
[13] V. Zwiller, H. Blom, P. Jonsson, N. Panev, S. Jeppesen, T. Tsegaye, E. Goobar, M.E. Pistol, L. Samuelson, G. Björk, Appl. Phys. Lett. 78 (2001) 2476.
[14] N. Akopian, N.H. Lindner, et al., Phys. Rev. Lett. 96 (13) (2006).
[15] R. Young, M. Stevenson, et al., New J. Phys. 8 (2) (2006) 29.
[16] R. Hafenbrak, S.M. Ulrich, et al., New J. Phys. 9 (9) (2007) 315.
[17] L. Goldstein, F. Glas, J.Y. Marzin, M.N. Charasse, G. Le Roux, Appl. Phys. Lett. 47 (1985) 1099.
[18] J.-Y. Marzin, J.-M. Gérard, A. Izraël, D. Barrier, G. Bastard, Phys. Rev. Lett. 73 (1994) 716–719.
[19] M.H.M. van Weert, N. Akopian, F. Kelkensberg, U. Perinetti, M.P. van Kouwen, L.P. Kouwenhoven, V. Zwiller, J. Gomez Rivas, M.T. Borgström, R.E. Algra, M.A. Verheijen, E.P.A.M. Bakkers, arXiv: 0808.2908v1 [cond-mat.mes-hall].
[20] R.S. Wagner, W.C. Ellis, Appl. Phys. Lett. 4 (1964) 89.
[21] E.I. Givargizov, J. Cryst. Growth 31 (1975) 20–30.
[22] M. Yazawa, M. Koguchi, A. Muto, M. Ozawa, K. Hiruma, Appl. Phys. Lett. 61 (1992) 2051.
[23] A.M. Morales, C.M. Lieber, Science 279 (1998) 208.
[24] M.T. Bjork, B.J. Ohlsson, T. Sass, A.I. Persson, C. Thelander, M.H. Magnusson, K. Deppert, L.R. Wallenberg, L. Samuelson, Appl. Phys. Lett. 80 (2002) 1058.
[25] Z.H. Wu, X.Y. Mei, D. Kim, M. Blumin, H.E. Ruda, Appl. Phys. Lett. 81 (2002) 5177.
[26] M.T. Borgström, G. Immink, B. Ketelaars, R. Algra, E.P.A.M. Bakkers, Nature Nanotechnol. 2 (2007) 541–544.
[27] F. Glas, J.-C. Harmand, G. Patriarche, Phys. Rev. Lett. 99 (2007) 146101.
[28] M.T. Borgstrom, M.A. Verheijen, G. Immink, T. de Smet, E.P.A.M. Bakkers, Nanotechnol. 17 (16) (2006) 4010–4013.
[29] M. Tchernycheva, G.E. Cirlin, G. Patriarche, L. Travers, V. Zwiller, U. Perinetti, J.-C. Harmand, Nano Lett. 7 (2007) 1500–1504.
[30] M. Yoshizawa, A. Kikuchi, M. Mori, N. Fujita, K. Kishino, Jpn. J. Appl. Phys. 36 (1997) L459.

[31] E. Calleja, M.A. Sanchez-Garcia, F.J. Sanchez, F. Calle, F.B. Naranjo, E. Munoz, S.I. Molina, A.M. Sanchez, F.J. Pacheco, R. Garcia, J. Cryst. Growth 201/202 (1999) 296.
[32] K. Ikejiri, J. Noborisaka, S. Hara, J. Motohisa, T. Fukui, J. Cryst. Growth 298 (2007) 616–619.
[33] J. Xiang, W. Lu, Y. Hu, Y. Wu, H. Yan, C.M. Lieber, Nature 441 (2006) 489–493.
[34] K.A. Dick, K. Deppert, M.W. Larsson, T. Mårtensson, W. Seifert, L.R. Wallenberg, L. Samuelson, Nature Mat. 3 (2004) 380.
[35] E.D. Minot, F. Kelkensberg, M. van Kouwen, J.A. van Dam, L.P. Kouwenhoven, V. Zwiller, M.T. Borgström, O. Wunnicke, M.A. Verheijen, E.P.A.M. Bakkers, Nano Lett. 7 (2) (2007) 367–371.
[36] Y.M. Niquet, D. Mojica, Phys. Rev. B 77 (11) (2008).
[37] C. Simon, Y.M. Niquet, X. Caillet, J. Eymery, J.P. Poizat, J.M. Gérard, Phys. Rev. B: Rapid Commun. 75 (2007) 081302.